ISME

Iranian Journal of Mechanical Engineering
The Iranian Society of Mechanical Engineers
Research Paper

DOI: 10.30506/JMEE.2022.121572.1224

Mechanical Behaviour of Femoral Diaphyseal Cortical Bone using the Computed Tomography Data: A Numerical Investigation

M. Mahmoudi[*]
M.Sc.

M. Salehi[†]
M.Sc.

F. Vatankhahan[‡]
M.Sc.

M.R. Dorali[§]
M.Sc.

H. Mahbadi[**]
Associate Professor

In this paper, mechanical behaviour and buckling analysis of human femoral bone are performed using the finite element method. A method is proposed to model the geometry and mechanical properties of Femur specimens. Mechanical properties of the bone are regarded both as homogeneous and nonhomogeneous quantities. Compressive tests are performed in three regions of the midshaft to validate the mechanical properties obtained by the CT scan. Waterjet cutting method is used to cut the samples which are used in compressive tests, and the 3D-printed models are used to locate the samples between the jaws of the test machine. Critical axial buckling loads of the femurs are studied, applying both of the homogeneous and nonhomogeneous material properties. Results show that the buckling load which is obtained by proposed homogenous modeling technique is close to the one which is obtained by nonhomogeneous modeling, and the proposed method is quite capable to simplify the FE analysis of the diaphyseal cortical bone.

Keywords: Diaphysis of Femur, Finite element method, Buckling analysis, Compressive test, Computed tomography scan, DXA, Nonhomogeneous modeling.

1 Introduction

Characterizing of the mechanical properties has an important role in Finite Element Analysis (FEA) of bones. Hounsfield Unit (HU) is a measured parameter by radiation attenuation through the bone tissues and may be used for characterizing the mechanical properties. The HU is commonly used to express the Computed Tomography (CT) numbers in a standardized and convenient form. Based on the CT data and HU, some equations are proposed for defining the isotropic and orthotropic material properties of bones [1, 2]. In recent years, there have been some studies on proximal Femur tissue by applying the finite element models with isotropic,

[*]Young Researchers and Elite Club, Central Tehran Branch, Islamic Azad University, Tehran, Iran, moeinoddin.mahmoudi@gmail.com
[†]Department of Mechanical Engineering, Islamic Azad University, Najafabad Branch, Najafabad, Iran, salehi.majid89@gmail.com
[‡]Department of Mechanical Engineering, Islamic Azad University, Najafabad Branch, Najafabad, Iran, fvatank@gmail.com
[§]School of Mechanical Engineering, College of Engineering, University of Tehran, P.O. Box 111554563, Tehran, Iran, m.r.dorali@ut.ac.ir
[**]Corresponding Author, Department of Mechanical Engineering, Central Tehran Branch, Islamic Azad University, Tehran, Iran, h_mahbadi@iauctb.ac.ir
Receive: 2020/02/11 Accepted: 2022/01/05

orthotropic, and anisotropic material properties [3–6]; however, the main complications regarding the orientation of the material properties along the non-uniform anatomy of bones remains. Although some researchers have used models with non-oriented orthotropic materials [7], oriented properties along a few anatomical directions corresponding to the bone shape has been used in most investigations [8]. Determined the oriented mechanical properties, some researches utilize the invasive methods such as slicing or crushing of bones [9].

Researches has been widely applied CT data to investigate the mechanical properties of bones which are required for 3-Dimensional (3D) modeling procedure through the FEA. Works regarding to the bone remodeling theory and interaction of bone and muscle [4], the evaluation of fracture risk and buckling analysis in tibia and fibula bones using the homogeneous mechanical properties, and the study of tensile and compressive loading along the sideways and longitudinal directions are among these biomechanical studies [10-14]. Assisted the FEA, stress analysis through the internal fixation of the tibia bone subjected to the 4-point bending and torsion is studied by researchers [15]. Besides, FEA adopted to analyze the stress shielding distribution in the Femur and internal fixation under static conditions by Naidubabu et al. [16]. CT scan data can separate the geometrical topology of cortical and trabecular tissues [7,17]. Quantitative Computed Tomography (QCT) is a medical method that measures Bone Mineral Density (BMD) by standard X-ray CT scanner devices and converts it to HU by a calibration standard [18]. Quantitative CT scans have been used to evaluate BMD at the lumbar spine [18], hip or femoral neck [3,7]. Generally, solid phantoms which are placed in a pad under the specimen during the CT image acquisition are used for calibration. BMD values of the specimen are detected by materials with various densities which are included in these phantoms [18]. Usually, either calcium hydroxyapatite (CaHAP) or dipotassium phosphate (K_2HPO_4) is used as the referenced standard [19]. Quantitative CT scan uses standardized software and phantom calibration to demonstrate the results in terms of areal BMD (mg/cm^2) of the trabecular vertebral (i.e. density within the measured region of interest). High correlations between QCT scan and spiral CT scan exists. This is due to the good correlations between HU values in CT scans and T-scores in DXA scans. Therefore, HU values are used for diagnosis of BMD diseases [20]. With the introduction of dual energy X-ray absorptiometry (DXA), application of QCT has been limited in clinical practice [18]. This is due to the long scanning time of QCT in comparison with DXA. In order to make use the HU value during the BMD assessment, phantomless or external reference phantoms are used to convert HU values to BMD [18,20]. Mechanical test (e.g. compressive test) is an alternative method which may be used to determine the bone mechanical properties. In this case, the cutting method which is used for sample preparation has an important role. Quality of cut surface using various cutting techniques including saw and waterjet method has been studied by many researchers (e.g. [21–24]). Study of this researches shows that waterjet cutting method is more appropriate for cutting of bones in comparison with direct contact methods (e.g. saw cutting method). This is due to the fact that less flaw and heat is imposed to the bone tissues by waterjet method.

Although the literature review shows application of CT data for determination of mechanical properties in bone tissues, few works address application of DXA and spiral CT data for modeling of human femoral diaphyseal cortical bone. Moreover, comparison between the mechanical properties of human femoral bone which are obtained by CT scan and those which are obtained by mechanical tests is rare in the literature. This paper utilizes DXA and CT scan data to determine the elastic modulus distribution of human femoral bone through its length. Alternatively, a compression test procedure is proposed to determine the elastic modulus of the bone through its various regions. The elastic modulus which is obtained by CT scan is compared with compression tests, and good agreement is achieved between the methods. To model the femoral diaphyseal cortical bone in FE software, CMM optical and CT scan are employed, and the axial critical buckling load of the bone is determined by FEA. Since FE modeling of the bone using the nonhomogeneous mechanical properties which are obtained by CT scan is

complicated, an effective method is proposed to determine the equivalent homogeneous elastic modulus of the bone which is required for FE modeling. To analyze the precision of the method, the critical buckling load which is obtained by homogenous modeling is compared with nonhomogeneous modeling.

2 Materials and methods

2.1 Bone mineral density

Three archeological human femoral bones were adapted in this investigation (with natural death). The main characteristics of human Femurs are given in Table (1). Specimens 1 and 2 were used for FEA, and specimen 3 was only used for compressive test. The human cadaveric femoral bones were cleaned of all soft tissues and articular cartilage. To prepare the specimens for the required tests of this study, they were kept in Formalin preservatives (Formaldehyde (HCHO) - according to pervious investigations [25]) at cool room temperature (i.e. +10°C). Examined by Spiral CT scan (Modern AZMA Co. Siemens - SOMATOM plus 4 in plain radiography with 46 kVp and 2.8 mAs), there were no fracture, cracks, defects as well as, no bone resorption in shaft-bone. The project were found to be in accordance to the ethical principles and the national norms and standards for conducting medical research in Iran by approval ID. IR.IAU.NAJAFABAD.REC.1397.004.

The dual energy X-ray absorptiometry (DXA) technique was applied for non-invasive estimation of the bone density. Norland DXA (XR-46 version) densitometer machine was used to estimate the gradient of density through the bone. The device meets the industry standards. The BMD test were carried out for the Femur specimens, and the corresponding results are shown in Figure (1) and Table (2). Figure (1) shows the contour of BMD test for neck, troch and wards of specimen 1. Table (2) shows that the osteoporosis of the Specimens 1 and 2 are 6.7% (Young Ref. 93.3%) and 14.8% (Young Ref. 85.2%), respectively (see Ref. [26] for Young Ref). Considering the age range, gender, and geographic location, the specimen 1 is in its lowest risk of fracture and its osteoporosis is equal to that of a healthy person and the second specimen is in its medium risk. In Table (2), value of Z-score is standard deviation of the osteoporosis with respect to a healthy person of the same age, and value of T-score is the standard deviation of osteoporosis with respect to a 30 years old healthy person of the same gender. Figure (1) shows the BMD contours using the DXA method for upper and lower parts of the specimen 1. This figure shows that the lowest density is 0.64 g/cm^2 at upper spongy area and the distal regions. The highest density is 1.95 g/cm^2 at cortical of the mid-shaft. The osteoporosis risk assessment data and BMD contours show that the specimens are completely healthy. The BMD contours will be used to obtain the mechanical properties of the bone which are required for FEA.

Table 1 Specification of human Femur specimens

Specimens	Side	Sex	Age	Weigh	Height
Specimen 1	Left	Male	44	85 (kg)	185 (cm)
Specimen 2	Left	Male	68	79 (kg)	189 (cm)
Specimen 3	Left	Male	53	81 (kg)	174 (cm)

Table 2 BMD results for specimens 1 and 2

Specimens	Region	BMD (g/cm^2)	Area (cm^2)	Length (cm)	T-Score	Z-Score	Young Ref. (%)
Specimen 1	Fem Neck	1.034	5.295	1.50	-0.59	0.49	93.3
Specimen 2	Fem Neck	0.872	4.662	1.50	-1.24	-0.24	85.2

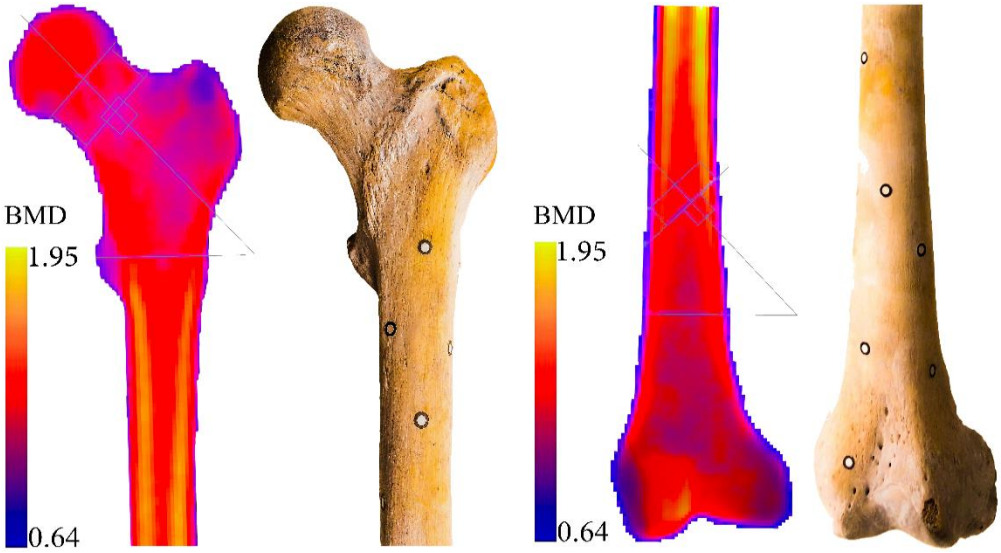

Figure 1 Result of the BMD through the proximal and distal of the specimen 1

2.2 Femoral diaphysis modeling

To periosteal margins modelling, specimens 1 and 2 were subjected to the 3D digital imaging. The optical coordinate measuring machine (CMM) was used for 3D imaging (optical CMM, made by GOM, Germany with VDA calibration). Using the point cloud digitization (i.e. STL and STEP files in CATIA V5/R21), the geometry of the bone was modeled as a shell (without central medullary cavity). Then, the model was converted to a solid model. It should be mentioned that the trabecular or marrow bones were not included in FE model. Figure (2) compares the bone surfaces which were modelled by CT data with those of optical CMM. This figure shows that triangular elements using CT data are much more than optical CMM. This is due to the fact that quality of the reconstructed surface by CT data is higher than optical CMM method. This conclusion is identical with Ref. [27]. So in this work, optical CMM method is applied to model the exterior region of the bone rather than CT data.
Figure (3)(1) shows the optical 3D scanning setup and results of optical CMM modeling without central cavity. Scanning was performed by the optical scanner on the movable stand and was controlled by the computer. To model the central cavity and endosteal area of the bones, we used the CT scan data (Spiral CT scan, modern AZMA Co. Siemens, SOMATOM, 120 kVp). Scanning parameters are slice spacing and scan energy with axial tomography and interpolation algorithm. Using the Marco PACS software, the bone was fully scanned through its diaphysis regions.

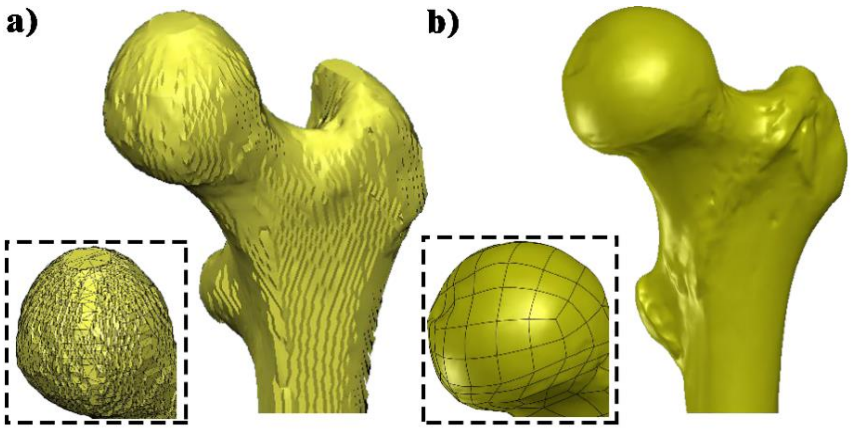

Figure 2 a) Mimics export using the CT scan modeling, b) SolidWorks export using the optical CMM modeling on outer surface.

The proximal and distal regions are not considered in this study. The absolute distance of each section from the top of the Femur was used to define the exact coordinate of the sections. All sections were stored as 2D images with Digital Imaging in Communication in Medicine (DICOM) format. The quality of 2D images were improved by Adobe Photoshop CC. Finally, the 3D model of the original Femur along with the 2D images of cross sections was transferred into SolidWorks 2013 software. Figure (3)(2) shows the created sketch of inner surface. In this figure, inner boundaries are determined by CT scan data. The exact boundaries of cross sections were used for this transformation as shown in Figure (3)(2). The cavities of the specimens were modeled using the lofted cut module of the software as shown Figure (3)(3). Since this article studies the critical buckling load of the bone shaft, the proximal and distal regions of Femur are excluded from the model. Figure (3)(4) shows the 3D model of the bone diaphysis with central cavity. The selected lengths of the femoral diaphysis are 230 mm and 260 mm for specimens 1 and 2, respectively. Using the variation of moment of inertia through the length of the bone, we have previously verified the proposed modeling technique for cortical bone [28].
Figure (4) shows the plot of cross-sectional area of diaphysis region versus the length of the femoral bone. As it can be seen from the figure, the cross sectional area decreases toward the end part of diaphysis. The maximum area is located at middle region of the bone shaft. Comparison of the cross sectional area with BMD results shows that the bone density has a direct relation with the area of the bone. Maximum bone density and maximum cross sectional area are almost located at the same distance.

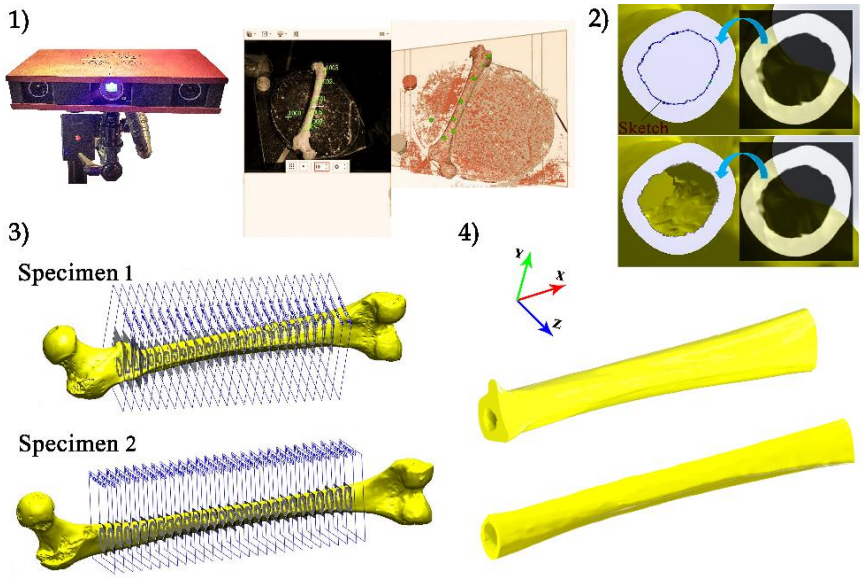

Figure 3 Bone diaphysis modeling using the optical CMM and CT data.

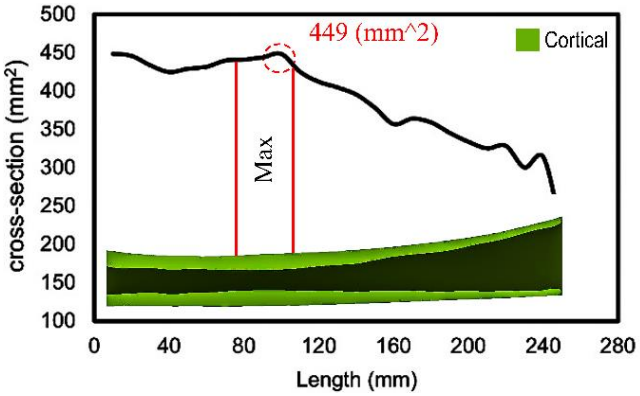

Figure 4 Plot of cross-sectional area with respect to the length of the whole-diaphysis cortical in specimen 1

2.3 Mechanical properties measurement

Utilized the CT data, this work models the elastic modulus of the bone both as homogeneous and nonhomogeneous isotropic materials. At first, the HU values are converted to the density (ρ_{QCT}). The following equation is proposed to evaluate the Femur density from HU values [19,20,29,30]:

$$\rho_{\mathrm{QCT}} = [0.859\ (\mathrm{HU}) - 2.38] \times 0.001 \quad (1)$$

The unit of density in this equation is g/cm^3. Then, the ash density ρ_{ash} (g/cm^3) is calculated for the femoral shaft. To this aim, the following equation is proposed [19,29].

$$\rho_{\mathrm{ash}} = 1.22\rho_{\mathrm{QCT}} + 0.0526 \quad (2)$$

The given equations in Table (3) are applied to calculate elastic modulus from the ash densaxity [7]. In this work, measured ash densities through all specimen regions are greater than 0.6.
So, the formula given in the last row of Table (3) is applied to convert the ash densities to the elastic modules.
To obtain the nonhomogeneous properties of specimens, HU is calculated per 23 sections of specimens 1 and per 26 sections of specimen 2. The HU value per section is obtained by averaging from HU over 100 points of the cross section. Figure (5)(2) shows the probe movement pattern which is used to evaluate the average HU for each cross section. As the figure shows, the selected points are located on an almost sinusoidal path. Selection of sinusoidal path results to depicting the points from three main areas which are located on the inner wall, the middle layer and the outer wall.
Plots of HU versus the length of the bones are shown in Figure (5)(3), and the average values of HU through the length of the specimens are specified on these plots. These values are 1686 and 1597 for specimens 1 and 2, respectively. Using Eq. (2), variations of ash density over the length of specimens 1 and 2 are plotted in Figure (6). Applying the equation given in last row of Table (3), the variation of elastic modulus over the length of the bone is determined. Average value of HU is employed to model the bone as a homogeneous material.
Accordingly, the average values of elastic modulus for specimens 1 and 2 are almost 34 GPa and 30 GPa, respectively. For specimen 1, minimum and maximum values of *E* are 21.5 GPa and 39.3 GPa, respectively. Also, for specimen 2, minimum and maximum *E* are 21.7 GPa and 37.7 GPa, respectively. As Figure 6 shows, the distance of maximum elastic modulus is located at 60 mm and 90 mm from top of the bone for specimens 1 and 2, respectively. The represented elastic modulus is employed in FE models for nonhomogeneous modeling. For homogeneous modeling, minimum, average and maximum values of *E* are imposed to the FE model.

Table 3 Material mapping methods using softer modulus-density relationship

Method	Modulus-Density relationship (MPa)	Densito-Metric range (g/cm^3)
NoShell	$E_0 = 6850 * \rho_{ash}^{1.49}$ [7]	All
Shell	$E_0 = 33900 * \rho_{\mathrm{ash}}^{2.20}$ [7]	$\rho_{\mathrm{ash}} \leq 0.27$
	$E_0 = 5307 * \rho_{\mathrm{ash}}$ interpolation [7]	$0.27 < \rho_{\mathrm{ash}} < 0.6$
	$E_0 = 10200 * \rho_{\mathrm{ash}}^{2.01}$ [2,7,17,29,31]	$\rho_{\mathrm{ash}} \geq 0.6$ [7]

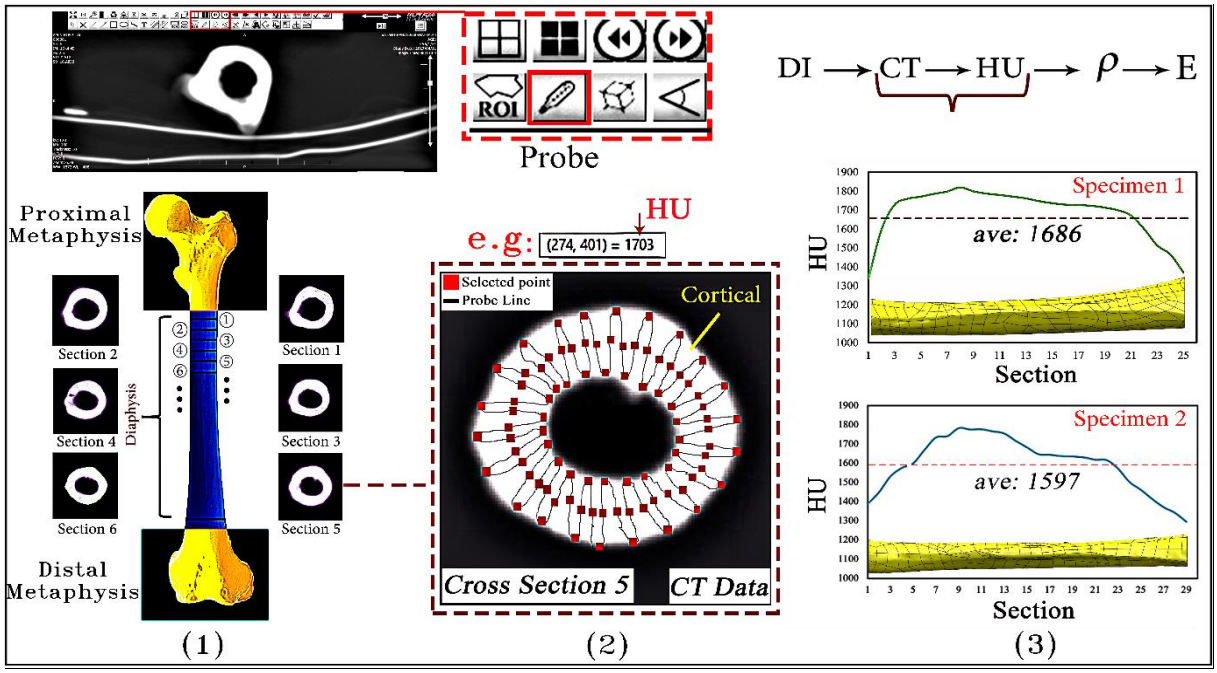

Figure 5 (1) And (2) HU calculating for each cross-section of CT data, and (3) is regression analyses HU/Section for cortical and for pooled groups (in specimens 1 and 2)

2.4 *Compressive test*

In this section, we alternatively obtain the elastic modulus of the bone by compressive test. To this aim, three specimens were cut from each of the specimens 1 and 3. Waterjet was used for cutting the specimen 1 and saw was used for cutting the specimen 3. The main advantage of waterjet is cutting of the bone without damaging and heat treating. Figure (7) shows cutting of the Femur using waterjet (American KMT waterjet system, SL-VI series pump). Figure 7(a) shows cutting of the sample by CNC waterjet machine using the nozzle distance of 0.92 mm and pressure of 50 MPa. Using this method, the cutting tolerance is 0.1 mm. Figure 7(b) shows the surface of the specimen after cutting. The quality of the cut surface is Q3 as shown in Figure 7(c). According to ASTM-E9 standard for compressive testing [32], the cut surfaces were subjected to electrical polishing to obtain the requirements of the compressive test. The length of specimens which were cut from specimens 1 and 3 are 70 mm and 30 mm, respectively. Figure (7) represents the location and cross-section of the cuts on specimens 1 and 3. The specified cross-sections correspond to beginning of the selected parts.

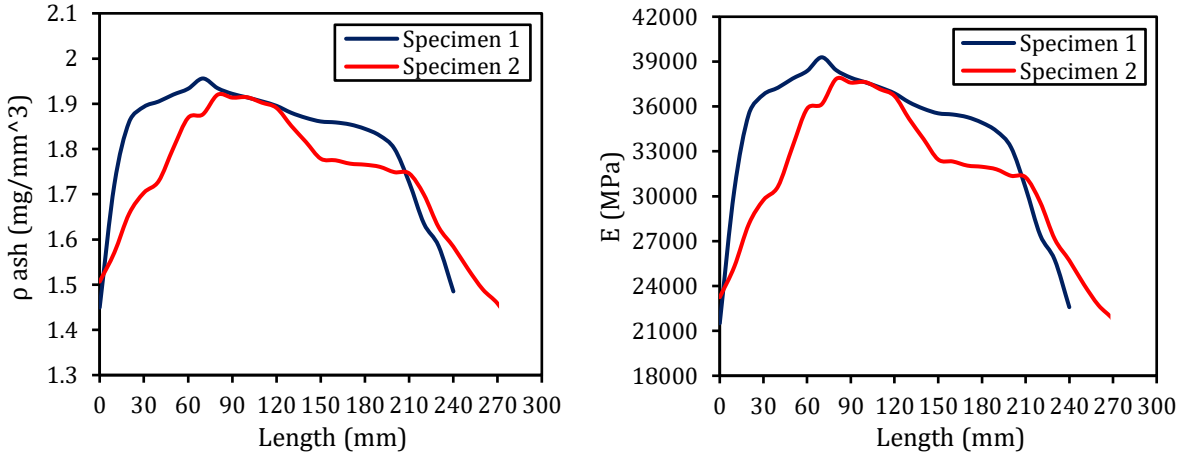

Figure 6 Plots of density and elastic modulus versus the length of the bone

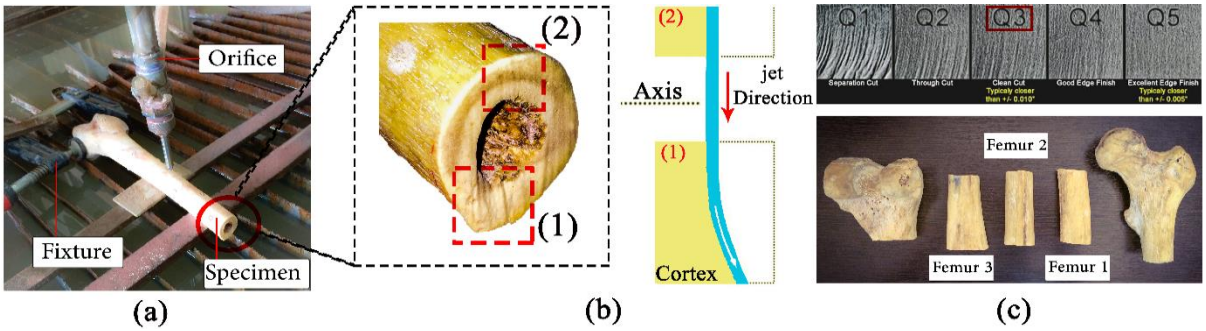

Figure 7 Orthogonal cutting of Femur using waterjet. (a) Fixing and cutting. (b) Surface of the sample after cutting and before polishing. (c) Quality of the cut surface, and Femurs 1, 2 and 3 in specimen 1

Figure (8) shows the setup which was used in this paper for compressive tests of the bone. The samples were located vertically in the GOTECH testing machine (servo control system universal testing machine: AI-7000 LA). The machine was calibrated and the applied preload was 10 kgf for each sample. Both ends of the specimen were fixed between the mandible and movable heads for all specimens (i.e. clamped-clamped conditions). The movable head moved down with speed of 4 mm/min for specimen 1 to eliminate the dynamic effects. The molds were designed using Punch & Matrix in CATIA V5/R21 software with 100×60×40 mm dimensions and 4 mm groove depth (fused deposition modeling (FDM) 3D printing method with Polylactic Acid (PLA) material). To fix both ends of the samples, the contact surfaces were covered with glue (glue Flex Tip); then samples were centered and placed vertically in the molds. The coefficient of the friction is almost zero on all contact surfaces (Figure 8b). Both molds were completely concentric and parallel to each other. Samples and molds were located between the jaws of the compression test system (the lower jaw was fixed and the upper jaw was movable) as shown in Figure 8(c). Distance between the two jaws was adjusted according to the length of the specimen. The load-displacement curves obtained during the compressive test were used to obtain the elastic modulus and compressive strength of the samples. Load was converted to the stress by average cross-section of the specimens. Applied the 3D modeling data, average cross-sections for specimens 1 and 3 are 385.96 mm^2 and 275.67 mm^2, respectively. Figure (9) shows the load-displacement curves which were converted to the stress-strain diagrams. The mechanical properties of the bone are specified from the stress-strain curve and are represented in Table (4) and Figure (10).

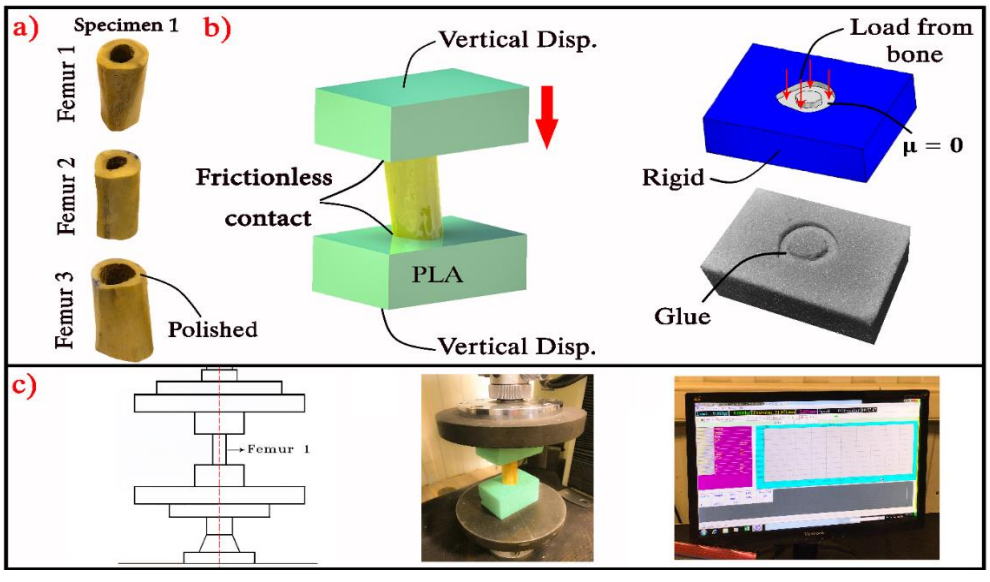

Figure 8 (a) Upper and bottom surfaces polishing of each sample, (b) the molds which are prepared by 3D printing from PLA material, (c) compressive test

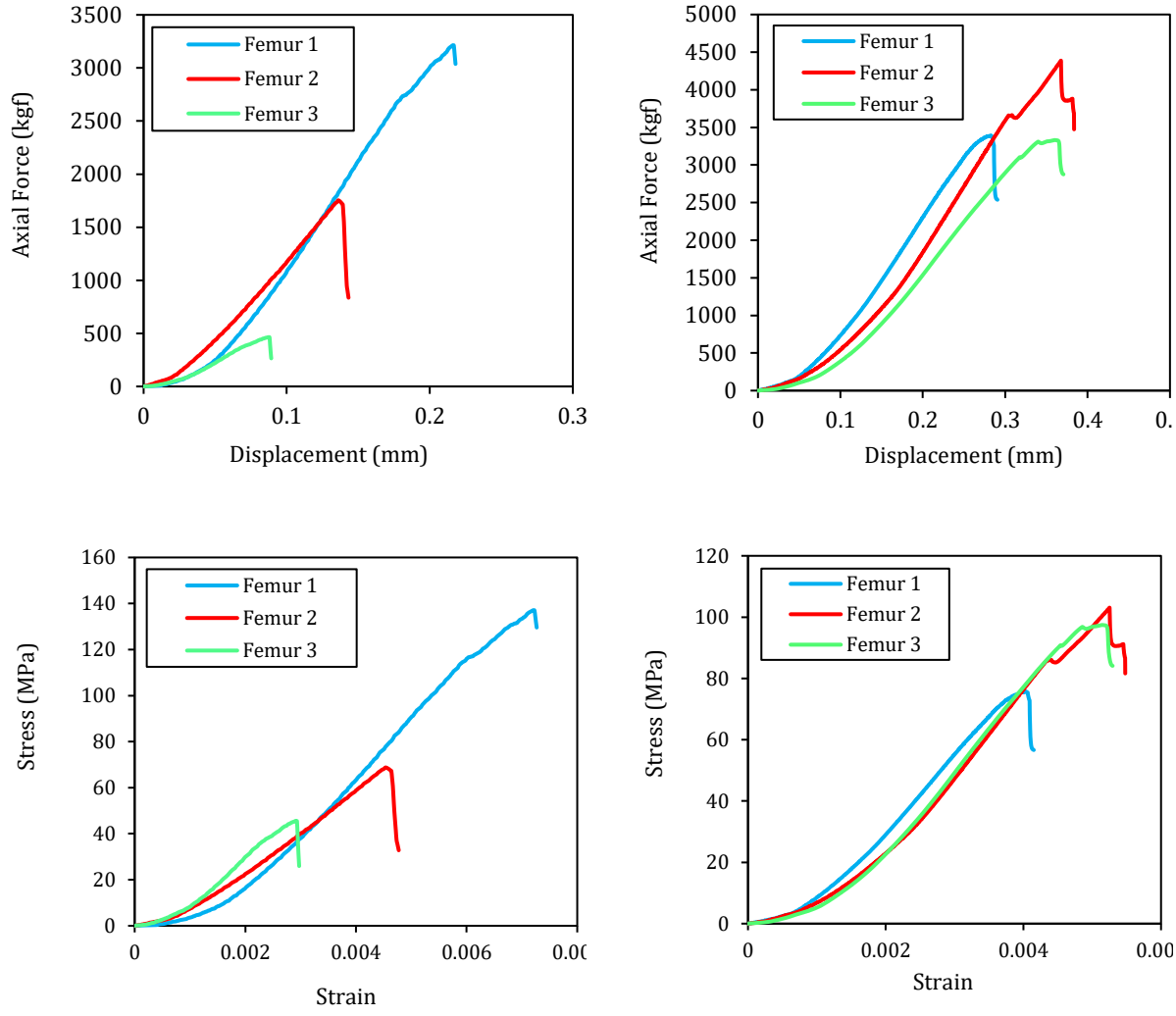

Figure 9 The load-displacement and stress-strain diagrams obtained from the tests, (a) specimen 3 and (b) specimen 1

obtained by compression test is almost 20% percent lower than the CT scan method. Curvature of the bone and application of the average cross sectional area are the main reasons for such difference. Elastic modulus which is determined by compressive test is between those of average and minimum values which are determined by CT scan method. Besides, the limitations of experimental procedure on the mechanical properties of bones under compressive load were the other reason.

Table 4 Elastic modulus and yield stress of cortical bone for Femur specimens obtained by compression test

Bone	**Specimen 3 (30 mm - Both ends fixed)**		**Specimen 1 (70 mm - Both ends fixed)**	
	Young's modulus (GPa)	Yield stress (MPa)	Young's modulus (GPa)	Yield stress (MPa)
Femur 1	25.50	137.04	26.40	75.76
Femur 2	17.50	68.80	29.00	103.10
Femur 3	22.60	45.53	28.00	96.80
Average	**21.86**	83.80	**27.80**	91.89

2.5 *Finite element simulation*

Applying the solid elements, the previous 3D models of the femoral diaphysis were meshed in ANSYS/Workbench software. Specimens 1 and 2 meshed with 156830 and 121070 quadratic tetrahedral elements C3D10 (with six degrees of freedom per node), respectively (Fig. 11a); the corresponding number of nodes in these specimens are 30145 and 23259 nodes. The 3-matic software was used to analyze and improve the quality of the elements. According to Fig. 11(b), displacements of the bone are modeled as fixed boundary condition on lower end (i.e. point A) and pined boundary condition on upper end (i.e. point B), respectively. The boundary conditions are U1=U2=U3=UR1=UR2=UR3=0 for fixed end and U2=U3=0 for pined end. A 30 kg static load was applied at center of the upper end (i.e. point C) of the bone for both specimens. The buckling analysis of the bone with mentioned loading and boundary condition were performed for both of the homogeneous and nonhomogeneous models. Figure 11(c) shows the nonhomogeneous model which was prepared for FEA. The figure shows the created partitions in diaphysis. The elastic modulus obtained by CT scan method was applied to each partition. In homogeneous FEA, three models based on minimum, average and maximum values of elastic modulus were prepared for buckling analysis. Poisson's ratio v was assumed to be 0.3.

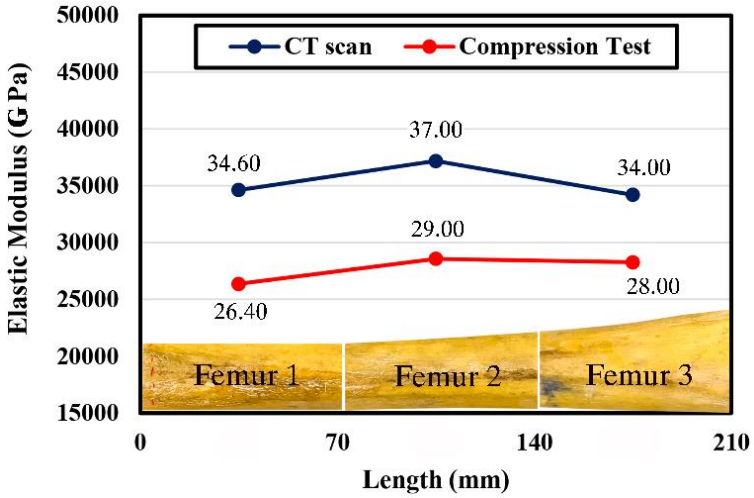

Figure 10 Comparison of elastic modulus obtained by CT scan and compression test (specimen 1)

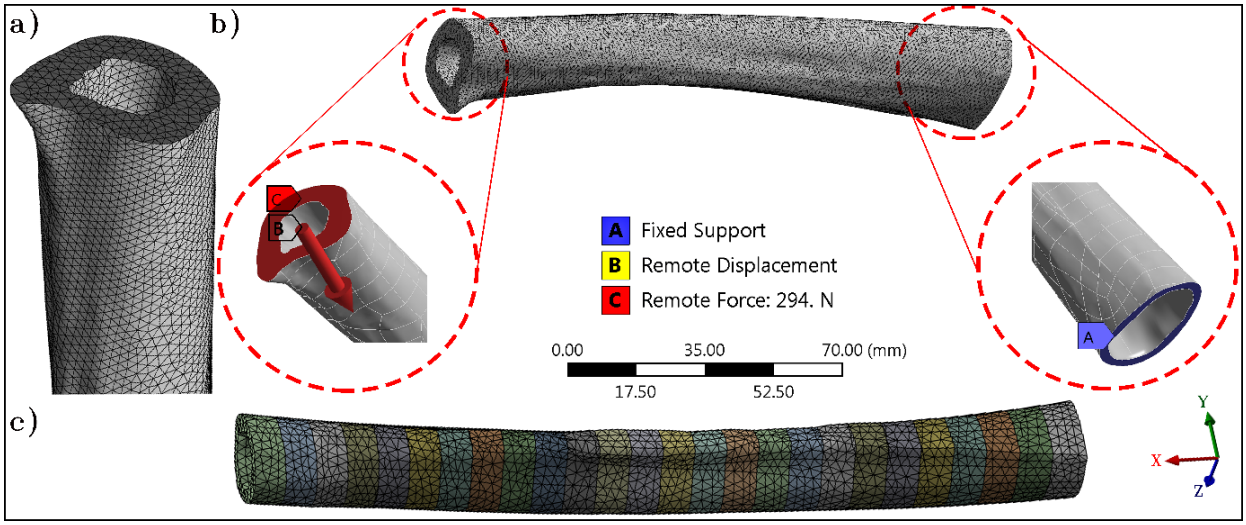

Figure 11 a) Bone meshing in specimen 1, b) boundary and loading conditions, c) partitions for specimen 2

3 Results and discussion

To obtain the critical axial buckling load of femoral diaphysis for the first and second modes, the created model in previous section is subjected to FEA. The buckling loads are determined using homogeneous and nonhomogeneous mechanical properties for both specimens. The critical buckling load which is determined by nonhomogeneous modeling are compared with homogenous modeling for specimens 1 and 2 (Table 5). Where the homogeneous modeling is applied, the critical buckling load is estimated based on the minimum, average and maximum values of the elastic modulus. The differences between the critical buckling loads which are obtained by homogenous and nonhomogeneous modeling are shown in Fig. 12. This figure shows that the critical buckling loads which is obtained by nonhomogeneous modeling are close to those of homogenous modeling with average elastic modulus. The difference in critical buckling load which is obtained by homogenous modeling with average elastic modulus is less than 4% and 0.4% with respect to nonhomogeneous modeling for specimens 1 and 2, respectively. Applied the nonhomogeneous analysis, Fig. 13 shows the first and second mode shapes of buckling for each specimen.

Table 5 Critical buckling load (kN) obtained by nonhomogeneous and homogeneous modeling in first and second modes

Models	Nonhomogeneous	Homogeneous		
		Min	Ave	Max
Specimen 1				
Mode 1	285.37	172.84	273.99	315.73
Mode 2	303.60	184.73	292.83	337.44
Specimen 2				
Mode 1	91.44	63.60	91.81	110.69
Mode 2	127.35	89.50	129.17	155.77

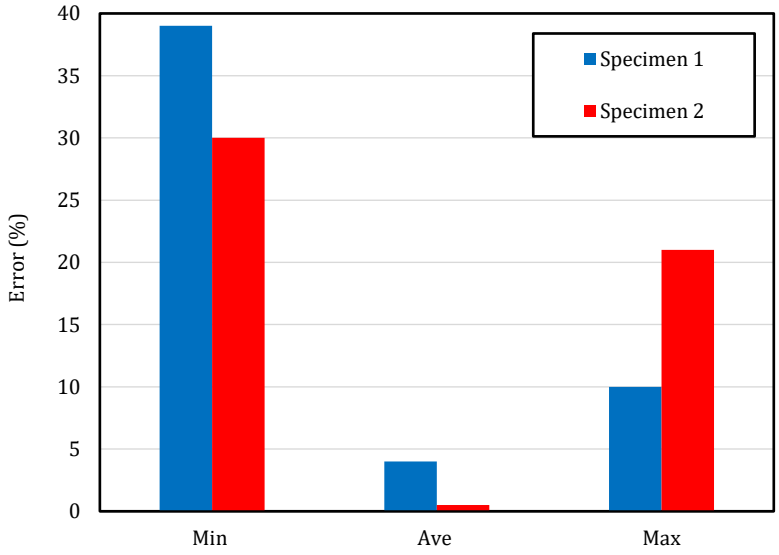

Figure 12 The difference in critical buckling loads which are obtained by homogenous modeling with minimum, average and maximum values of *E* with respect to nonhomogeneous modeling in first mode

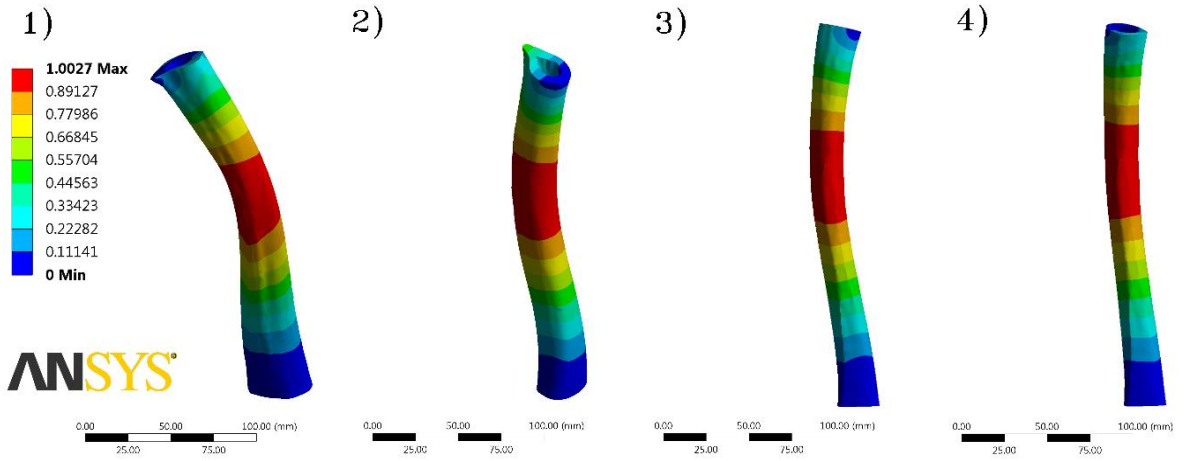

Figure 13 First and second buckling mode shape obtained by nonhomogeneous modeling of the specimens 1 and 2. 1) Mode 1 specimen 1, 2) mode 2 specimen 1, 3) mode 1 specimen 2 and 4) mode 2 specimen 2

On the other hand, the Euler formula (Eq. 3) may be applied to determine the buckling load of a homogeneous beam with uniform cross section. That is

$$P_{cr} = \frac{\pi^2 EI}{(CL)^2} \tag{3}$$

where C is 0.7 for clamped-simply supported boundary conditions, L is length of the Femur diaphyseal, I is the moment of inertia, and E is the elastic modulus. Regarding the results of elastic modulus, cross-sections as well as lengths of the bones, it was expected that the critical buckling loads in the specimen 2 would be lower than the specimen 1. The average moments of inertia for specimens 1 and 2 are $1.877 * 10^{-8}$ and $1.138 * 10^{-8}$, respectively. These values are calculated based on the average cross sectional area of the diaphysis. Applying the Euler formula, the obtained critical buckling loads for specimens 1 and 2 are 248 kN and 107.6 kN, respectively. Compared to FEA with homogenous mechanical properties (i.e. applying the average elastic modulus), these values are 9.5% lower and 17% larger for specimens 1 and 2, respectively. This results validate the FEA.

4 Conclusion

The DXA method and CT data are applied to FE modeling of femoral bone as a nonhomogeneous material. The elastic modulus obtained by CT scan is compared with those obtained by compressive testing of the bone. The results between these two methods are well compared and show that the CT scan is applicable to obtain the mechanical properties of the bone. The geometry of the bone is accurately modeled using the optical CMM and CT data, and the critical buckling load of the bone is obtained by FEA. The critical buckling load in FEA is obtained for both cases of homogeneous and nonhomogeneous modeling of the bone. Where the homogenous model with average elastic modulus is applied, the critical buckling load of homogenous and nonhomogeneous models are very close to each other. Comparison of various methods of modeling and validation of results with Euler formula indicate that the proposed method may be applied to FEA of the bone. While accuracy of the result is acceptable, the modeling procedure is simplified by proposed homogenous modeling procedure. In summary, the methods presented in this paper are considered to be a more traditional method for modeling the geometry and mechanical properties of bone in comparison with the current state of knowledge and the latest available high technologies. But in this way, where there is lack of precise methods and instruments for modeling and simulation of the bone, this method may be used for FEA of bones with an acceptable error.

Acknowledgments

We would like to thank Dr. Saman Zamani for CT data analyzing and also Islamic Azad University of Central Tehran Branch for research funding, Amin medical center (department of medical imaging and Spiral CT scan), Shohada research and medical department, Razi applied science foundation, Islamic Azad University of Najafabad Branch (moulage laboratory, advanced materials research center, molding and casting workshops), Foolad Bon and Nano Optic companies.

Competing interests
There is no competing interests regarding this manuscript.

Funding
This project was funded by the Islamic Azad University of Central Tehran Branch (IAUCTB).

References

[1] Peng, L., Bai, J., Zeng, X., and Zhou, Y., "Comparison of isotropic and orthotropic material property assignments on femoral finite element models under two loading conditions", Med Eng Phys, Vol. 28, pp. 227-233, (2006).

[2] Trabelsi, N., and Yosibash, Z., "Patient-specific finite-element analyses of the proximal femur with orthotropic material properties validated by experiments", Journal of Biomechanical Engineering, 133, (2011).

[3] Zysset, P., Pahr, D., Engelke, K., Genant, H.K., McClung, M.R., Kendler, D.L., Recknor, C., Kinzl, M., Schwiedrzik, J., Museyko, O., Wang, A., and Libanati, C., "Comparison of proximal femur and vertebral body strength improvements in the FREEDOM trial using an alternative finite element methodology", Bone, Vol. 81, pp.122-130, (2015).

[4] Mathukumar, S., Nagarajan, V.A., and Radhakrishnan, A., "Analysis and validation of femur bone data using finite element method under static load condition", Proc IMechE Part C: J Mechanical Engineering Science, Vol. 233(16), pp. 5547-5555, (2019).

[5] Amini, M., Nazemi, S.M., Lanovaz, J.L., Kontulainen, S., Masri, B.A., Wilson, D.R., Szyszkowski, W., and Johnston, J.D., "Individual and combined effects of OA-related subchondral bone alterations on proximal tibial surface stiffness: A parametric finite element modeling study", Med Eng Phys, Vol. 37, pp. 783-791, (2015).

[6] Enns-Bray, W.S., Owoc, J.S., Nishiyama, K.K., and Boyd, S.K., "Mapping anisotropy of the proximal femur for enhanced image based finite element analysis", J Biomech, Vol. 47, pp. 3272-3278, (2014).

[7] Enns-Bray, W.S., Ariza, O., Gilchrist, S., Widmer Soyka, R.P., Vogt, P.J., Palsson, H., Boyd, S.K., Guy, P., Cripton, P.A., Ferguson, S.J., and Helgason, B., "Morphology based anisotropic finite element models of the proximal femur validated with experimental data", Med Eng Phys, Vol. 38, pp. 1339-1347, (2016).

[8] San Antonio, T., Ciaccia, M., Müller-Karger, C., and Casanova, E., "Orientation of

orthotropic material properties in a femur FE model: A method based on the principal stresses directions", Med Eng Phys, Vol. 34, pp. 914–919, (2012).

[9] Varga, P., Schwiedrzik, J., Zysset, P.K., Fliri-Hofmann, L., Widmer, D., Gueorguiev, B., Blauth, M., and Windolf, M., "Nonlinear quasi-static finite element simulations predict in vitro strength of human proximal femora assessed in a dynamic sideways fall setup", J Mech Behav Biomed Mater, Vol. 57, pp. 116-127, (2016).

[10] van de Laarschot, D.M., and Zillikens, M.C., "Atypical femur fracture in an adolescent boy treated with bisphosphonates for X-linked osteoporosis based on PLS3 mutation", Bone, Vol. 91, pp. 148-151, (2016).

[11] Voo, L., Armand, M., and Kleinberger, M., "Stress fracture risk analysis of the human femur based on computational biomechanics", JOHNS HOPKINS APL Tech Dig, Vol. 25(3), pp. 223-230, (2004).

[12] Mahmoudi, M., Amini, S., Vatankhahan, F., and Mahbadi, H., "Buckling analysis of human Tibia and Fibula bones", 25th Annual International Conference on Mechanical Engineering, Tarbiat Modares University, Tehran, Iran. April 16-18, (2017).

[13] Mahmoudi, M., Vatankhahan, F., Salehi, M., and Mahbadi, H., "Experimental investigation of compressive strength in diaphysis of human Tibia and Fibula bones", 25th Annual International Conference on Mechanical Engineering. Tarbiat Modares University, Tehran, Iran. April 16-18, (2017).

[14] Havaldar, R., Pilli, S.C., and Putti, B.B., "Insights into the effects of tensile and compressive loadings on human femur bone", Adv Biomed Res, 3:101, (2014).

[15] Avery, C.M.E., Bujtár, P., Simonovics, J., Dézsi, T., Váradi, K., Sándor, G.K.B., and Pan, J., "A finite element analysis of bone plates available for prophylactic internal fixation of the radial osteocutaneous donor site using the sheep tibia model", Med Eng Phys, Vol. 35, pp. 1421-1430, (2013).

[16] Naidubabu, Y., Mohana Rao, G., Rajasekhar, K., and Ratna Sunil B., "Design and simulation of polymethyl methacrylate-titanium composite bone fixing plates using finite element analysis: Optimizing the composition to minimize the stress shielding effect", Proc IMechE Part C: J Mechanical Engineering Science, Vol. 231(23), pp. 4402-4412, (2017).

[17] Morgan, E.F., Bayraktar, H.H., and Keaveny, T.M., "Trabecular bone modulus-density relationships depend on anatomic site", J Biomech, Vol. 36, pp. 897-904, (2003).

[18] Batawil, N., and Sabiq, S., "Hounsfield unit for the diagnosis of bone mineral density disease: A proof of concept study", Radiography, Vol. 22, pp. e93-98, (2016).

[19] Faisal, T.R., and Luo, Y., "Stress variations owing to single-stance load and sideways fall result in fracture at proximal femur", Proceedings - International Symposium on Biomedical Imaging, (2015).

[20] Knowles, N.K., Reeves, J.M., and Ferreira, L.M., "Quantitative computed tomography (QCT) derived Bone Mineral Density (BMD) in finite element studies: a review of the literature", J Exp Orthop, 3:36, (2016).

[21] den Dunnen, S., Dankelman, J., Kerkhoffs, G.M.M.J., and Tuijthof, G.J.M., "How do jet time, pressure and bone volume fraction influence the drilling depth when waterjet drilling in porcine bone?", J Mech Behav Biomed Mater, Vol. 62, pp. 495-503, (2016).

[22] den Dunnen, S., Mulder, L., Kerkhoffs, G.M.M.J., Dankelman, J., and Tuijthof, G.J.M., "Waterjet drilling in porcine bone: The effect of the nozzle diameter and bone architecture on the hole dimensions", J Mech Behav Biomed Mater, Vol. 27, pp. 84-93, (2013).

[23] Kraaij, G., Tuijthof, G.J.M., Dankelman, J., Nelissen, R.G.H.H., and Valstar, E.R., "Waterjet cutting of periprosthetic interface tissue in loosened hip prostheses: An in vitro feasibility study", Med Eng Phys, Vol. 37, pp. 245-250, (2015).

[24] Wang, J., and Shanmugam, D.K., "Cutting meat with bone using an ultrahigh pressure abrasive waterjet", Meat Sci, Vol. 81, pp. 671-677, (2009).

[25] Zhang, G., Wang, S., Xu, S., Guan, F., Bai, Z., and Mao, H., "The Effect of Formalin Preservation Time and Temperature on the Material Properties of Bovine Femoral Cortical Bone Tissue", Annals of Biomedical Engineering, (2019).

[26] Boehm, H.F., Horng, A., Notohamiprodjo, M., Eckstein, F., Burklein, D., Panteleon, A., Lutz, J., and Reiser, M., "Prediction of the fracture load of whole proximal femur specimens by topological analysis of the mineral distribution in DXA-scan images", Bone, Vol. 43, pp. 826-831, (2008).

[27] Soodmand, E., Kluess, D., Varady, P.A., Cichon, R., Schwarze, M., Gehweiler, D., Niemeyer, F., Pahr, D., and Woiczinski, M., "Interlaboratory comparison of femur surface reconstruction from CT data compared to reference optical 3D scan", BioMedical Engineering OnLine, 2;17(1):29, (2018).

[28] Mahmoudi, M., Dorali, M.R., Heydari Beni, M., and Mahbadi, H., "Bio-CAD modeling of femoral bones with Dual X-ray absorptiometry and Spiral CT-scan technique", The 26th Annual International Conference of Iranian Society of Mechanical Engineers. Semnan University, Semnan, Iran. 24-26 April, (2018).

[29] Alavi, F., and Mirzaei, M., "Experimental and Computational Analysis of Fracture Load and Pattern of Human Femur using Cohesive Zone Model", Modares Mechanical Engineering, Vol. 15(10), pp. 192-200, (2015), (In Persian).

[30] Schileo, E., Dall'Ara, E., Taddei, F., Malandrino, A., Schotkamp, T., Baleani, M., and Viceconti, M., "An accurate estimation of bone density improves the accuracy of subject-specific finite element models", J Biomech 41, pp. 2483-91, (2008).

[31] Helgason, B., Gilchrist, S,. Ariza, O., Vogt, P., Enns-Bray, W., Widmer, R.P., Fitze, T., Pálsson, H., Pauchard, Y., Guy, P., Ferguson, S.J., and Cripton, P.A., "The influence of the modulus-density relationship and the material mapping method on the simulated mechanical response of the proximal femur in side-ways fall loading configuration", Med Eng Phys, Vol. 38, pp. 679-689, (2016).

[32] Kemper, A., McNally, C., Kennedy, E., Manoogian, S., and Duma, S., "The material properties of human tibia cortical bone in tension and compression: implacations for the tibia index", Paper Number 07-0470.

[33] Wang, X., Nyman, J.S., Dong, X., Leng, H., and Reyes, M., "Fundamental Biomechanics in Bone Tissue Engineering", Morgan & Claypool, (2010).